IET Research Journals

Research Article

IET Journals
The Institution of Engineering and Technology

Droop-Free Hierarchical Control Strategy for Inverter-Based AC Microgrids

ISSN 1751-8644
doi: 0000000000
www.ietdl.org

Juan M. Rey[1], Pedro P. Vergara[2], Miguel Castilla[3], Antonio Camacho[4], Manel Velasco[5], Pau Martí[5]

[1] *Escuela de Ingenierías Eléctrica, Electrónica y de Telecomunicaciones (E3T), Universidad Industrial de Santander (UIS), Bucaramanga 680002, Colombia.*
[2] *Electric Energy Systems (EES) Group, Department of Electrical Engineering, Eindhoven University of Technology, Eindhoven 5600 MB, The Netherlands.*
[3] *Department of Electronic Engineering, Technical University of Catalonia (UPC), Vilanova i la Geltrú 08800, Spain.*
[4] *Department of Automatic Control, Technical University of Catalonia (UPC), Vilanova i la Geltrú 08800, Spain.*
[5] *Department of Automatic Control, Technical University of Catalonia (UPC), Barcelona 08028, Spain.*
* *E-mail: juanmrey@uis.edu.co*

Abstract: Hierarchical schemes are widely used for the design of inverter-based AC microgrids control strategies. To ensure a reliable operation, hierarchical control must consider together all the functionalities that allow the regulation of key variables and guarantee a safe transition between operation modes. Conventionally, in the literature are proposed three-layer schemes which present relevant drawbacks: they include limited functionalities and they use droop method for the primary layer which, despite its decentralized nature, suffers from issues that have motivated the development of alternative strategies. Considering this, the contribution of this paper is twofold. First, a droop-free hierarchical control strategy that satisfy a proper operation of AC microgrids is proposed. Control objectives such as power-sharing, frequency regulation, optimal power dispatch, and voltage regulation are considered. Second, a closed-loop small-signal model, which facilitates the control parameters design and fills a gap in the literature is presented. Differences between the proposal and previous controls are discussed. Selected tests are carried out in a laboratory microgrid under different conditions, including normal operation and the response to failures in the central controller and to communication impairments. The experimental results show a good performance of the proposal even in adverse conditions.

1 Introduction

The design of control strategies for microgrids (MGs) is commonly based on hierarchical approaches. These control structures are characterized by dividing the variables and control objectives of a system in layers, according to their expected dynamics [1–3]. For microgrids operation, a three-layer scheme is widely used as follows: the primary layer (commonly using the droop method) regulates the local frequencies on each distributed generator (DG) until a MG global frequency is reached, achieving also an appropriate power-sharing [4]. The deviations produced on variables as frequency and local voltage magnitudes are restored by the secondary layer. Finally, with the slowest time of response, the tertiary layer coordinates the power dispatch based on economical and operational constraints [5–7].

Beyond these standard control objectives, within the framework of hierarchical control other critical functionalities must be considered for the proper operation of MGs. This is the case of monitoring and control of the point of common coupling (PCC), the node of the MG where the connection to the main grid is made. This point is critical for permanently guarantee a safe transition from islanded mode to grid-connected mode (avoiding high power overshoots and undesired current and voltage peaks). Although being able to execute this transition between modes of operation is a fundamental feature to improve the reliability of microgrids, many proposals fail in omit this control objective in the hierarchical control.

It is possible to identify in the literature several hierarchical control strategies proposed with the aim of fulfilling some of the control objectives discussed above [8–34]. For instance, in [8–21] multi-layer hierarchical control schemes are proposed guaranteeing power sharing and frequency regulation. The strategies in [8–17] focuses exclusively on the primary and secondary layers and its control objectives. On them, the primary layer is based on the droop method and the secondary control layer is designed to restore the deviations using centralized [8], distributed [9–15] and communicationless techniques [16, 17]. In [18–21] a synchronization loop is included in order to control the connection of the MG to the grid by modifying the references of the secondary layer. However, these proposals do not consider the optimal dispatch of the DGs, whose inclusion may not be trivial.

Other proposals, as the presented in [22–29], are characterized by including an optimal power dispatch in the hierarchical control structure. In these works, the result obtained is a reduction in the total generation cost compared with similar control schemes. Although they include different control objectives, none considers any type of PCC voltage regulation mechanism. Only a few works consider this functionality, usually focusing on the fulfillment of this control objective and omitting others. This is the case of the work presented in [30], in which a control for voltage quality enhancement on a selected bus is presented. As discussed, it is not usual for hierarchical control proposals to include all the necessary features to guarantee a reliable operation of the microgrid.

Another important aspect about the references cited above (i.e., [8–30]), is that they all base the primary layer on the droop control. In this control method, the virtual inertia guarantees a unique global frequency of operation and a good power-sharing without requiring communication among the DGs controllers. However, it is well known that droop control suffers from relevant drawbacks such as a strong dependence on the nature of the loads that produce important frequency/voltage deviations, control loops coupling issues in the presence of resistive-inductive grid impedances, and performance impairments in non-linear loads scenarios [33].

The aforementioned issues have motivated the development of alternative control strategies based on principles other than the standard droop control [31–34]. In [31] and [32], local controllers are designed to track optimized set points. Moreover, in [33] and [34], cooperative distributed control strategies have been proposed satisfying both primary and secondary control layers objectives. These proposals offer good dynamic performance. However, they do not consider the control of the voltage at PCC. Furthermore, the lack of

a power dispatch mechanism impedes optimal management of the operation and generation costs [7].

In Table 1 the characteristics of the discussed works are presented. Note that there are no hierarchical control strategies based on principles different from those of standard droop control, capable of simultaneously guaranteeing objectives for MGs operation such as: active and reactive power sharing, frequency regulation, optimal power dispatch and voltage regulation at the PCC. Motivated by the aforementioned research gap, a droop-free hierarchical control strategy for inverter-based MGs with optimal power dispatch and PCC voltage regulation is presented. The contribution of this paper is twofold:

1. It presents and describes a hierarchical control strategy with the characteristics previously exposed that exhibits good performance in terms of control objectives accomplishment and dynamics properties.
2. It provides a small-signal closed-loop system model that fills an existing gap in the state-of-the-art of MG modeling. The model is used for the control parameters design to guarantee MG stability.

To analyze and evaluate the performance of the proposed control, multiple experimental tests are carried out in a laboratory microgrid under different conditions. The selected tests include: normal operation and the response to failures in the central controller and to communication impairments

The remainder of this paper is organized as follows. In Section 2, the strategic methodology that will be followed in the paper is presented. In Section 3, the operation modes of the MG are characterized. In Section 4, the control objectives are formulated. In Section 5, metrics for the performance evaluation are stated. In Section 6, the proposed control strategy is presented. In Section 7, the system modeling is described and in Section 8 the control parameters design is discussed. Selected experimental results to validate the proposal are presented and discussed in Section 9. Finally, conclusions are drawn in Section 10.

2 Strategic methodology

In this Section, the strategic methodology that will be followed to present the control proposal is described. This methodology is inspired by the process of strategic planning, a method commonly used to design strategies for multiple applications and work fields, that seeks to guarantee the properly accomplishment of a series of predefined objectives [35, 36]. The methodology includes three main steps: formulation, design and evaluation. A general scheme of it is shown in Fig. 1.

2.1 General description

Formulation: The strategic formulation starts with an operational characterization of the application, in this case, the MGs operation modes. The objective is to identify the differences that exist in each mode, their particularities as well as the desired technical features, in order to establish the control objectives and define performance evaluation metrics. These aspects will be discussed and presented in Sections 3, 4 and 5.

Table 1 Comparison of hierarchical control strategies

Ref.	Power sharing	Frequency regulation	Optimal dispatch	PCC regulation	Alternative to droop
[8–17]	✓	✓	✗	✗	✗
[18–21]	✓	✓	✗	✓	✗
[22, 23]	✓	✗	✓	✗	✗
[24–29]	✓	✓	✓	✗	✗
[30]	✗	✗	✗	✓	✗
[31–34]	✓	✓	✗	✗	✓
Proposed control	✓	✓	✓	✓	✓

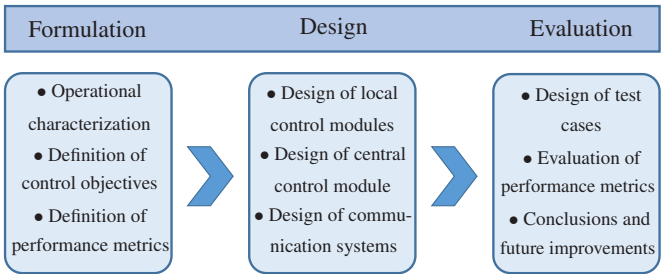

Fig. 1: Strategic methodology scheme.

Design: The next step is to design the control strategy which requires a detailed description of the local and central control modules, control equations, implementation aspects and the communication framework that support the strategy operation. Also, a complete modeling should be provided to determine design guidelines for the control parameters. These aspects are developed in Sections 6, 7 and 8.

Evaluation: The evaluation is the last step, which requires a proper design of test cases in order to know if the components and the whole strategy are working correctly. To achieve this, performance metrics should be calculated being the basis to obtain conclusions and visualize future improvements. This is addressed in Sections 9 and 10.

3 Operational characterization

The first step to design control strategies for MGs, is to properly characterize the operation modes (islanded and grid-connected) and its technical features aiming to identify the most relevant aspects that define the desired operation.

In islanded mode, MGs work disconnected from the main grid. The absence of a dominant electrical reference represents a major control challenge. On the one hand, as the frequency is not imposed by a dominant system, it is necessary to ensure an adequate frequency regulation using at least one element of the MG as reference generator or designing a control strategy that does not operate based on frequency deviations (i.e., contrary to the droop method case). On the other hand, the possibility to operate isolated is a potential scenario to supply the demanded local load consumption optimizing the power dispatch according to economical variables.

An important aspect of the islanded mode, is that the intermittent nature of the renewable energy sources represents a limitation and a risk for the reliability of the power supply. For this reason, whenever possible, it is highly recommended to provide the MGs with mechanisms that allow the connection to the main grid guaranteeing a safety synchronization of the critical values at the PCC. Once the MG is functioning in grid-connected mode, the presence of a dominant electrical reference guarantees the frequency regulation while the MG control can be used to execute auxiliary functions related to power quality and voltage control.

The previous discussion allows to conclude about the key control objectives that must be considered to design a control strategy ensuring an adequate response to realistic operational scenarios. From a general perspective, the proposed control strategy has as objective (mission) controlling the operation of inverter-based AC microgrids integrating different types of control modules, communication systems and functionalities to guarantee a simultaneously fulfillment of goals related to the optimal operation and the safe transition between operation modes. To achieve this, the following actions are going to be considered:

• To ensure the frequency regulation (key to achieve an adequate operation performance in isolated mode and to guarantee a good synchronization with the main grid) the control strategy will be based on a droop-free hierarchical structure. This type of control scheme does not require frequency deviations to operate, allowing the MG to work at nominal frequency in almost all the possible operation scenarios.

• To ensure an optimal operation of the MG, the strategy must be able to dispatch the active and reactive powers of the controllable DGs considering operational constraints and power availability. Based on this, the active and reactive power sharing as well as the optimal power dispatch will be considered as control objectives .
• To ensure a safe transition between operation modes, the strategy must include a grid synchronization mechanism in order to adjust the key electrical variables of the PCC.

The next step of strategy formulation consists of mathematically describe the control objectives and determine the evaluation metrics that are going to be used in the evaluation stage. This is presented in the following sections.

4 Definition of the control objectives

The control objectives of the proposed control strategy can be formulated for the set of N DGs as follows:

Control objective (a): Active and reactive power sharing control. It can be expressed as

$$\frac{P_1}{P_1^D} = ... = \frac{P_i}{P_i^D} \quad \forall\, i \in N \tag{1}$$

$$\frac{Q_1}{Q_1^D} = ... = \frac{Q_i}{Q_i^D} \quad \forall\, i \in N \tag{2}$$

where P_i and Q_i are the active and reactive powers injected by the i^{th} DG, and P_i^D and Q_i^D are their optimal dispatched references.

Control objective (b): Optimal power dispatch. It can be defined as an optimization problem in which the objective function $f(X)$ is minimized over the set of control variables X, as follows

$$\min\{f(X)\} \qquad \text{subject to: } h(X) = 0;\ g(X) \leq 0 \tag{3}$$

being $h(X)$ and $g(X)$ the operational and technical constraints. The objective function $f(X)$ is the generation cost function using P_i^D and Q_i^D as the decision variables.

Control objective (c): Voltage regulation at the PCC. It can be formulated as

$$V_{PCC} = V_0 \tag{4}$$

where V_{PCC} is the voltage amplitude at the PCC and V_0 is the voltage reference.

5 Performance evaluation metrics

In this Section, performance evaluation metrics are presented which are related to the control objectives previously stated. Its formulation is intended for steady-state variables and for this reason its calculation makes sense only when the variables are stabilized.

Control objective (a): According to (1) the error of the active power sharing for the i^{th} DG can be defined as

$$e_i^{PS}(\%) = \frac{\left| \frac{P_i}{P_i^D} - \frac{1}{N}\sum_{j=1}^{N} \frac{P_j}{P_j^D} \right|}{\frac{1}{N}\sum_{j=1}^{N} \frac{P_j}{P_j^D}} 100. \tag{5}$$

Similarly, according to (2) and replacing the active powers by reactive powers in (5), the error of the reactive power sharing for the i^{th} DG (e_i^{QS}) can be calculated.

Control objective (b): The accuracy of the dispatch implementation of the i^{th} DG is evaluated considering the active power dispatch error e_i^{PD} as

$$e_i^{PD}(\%) = \frac{\left| P_i - P_i^D \right|}{P_i^D} 100. \tag{6}$$

Similarly, replacing the active powers by reactive powers in (6), the reactive power dispatch error for the i^{th} DG (e_i^{QD}) can be calculated.

Control objective (c): According to the control objective stated in (4), the voltage error can be defined as

$$e^V(\%) = \frac{|V_{PCC} - V_0|}{V_0} 100. \tag{7}$$

These metrics will serve to evaluate the performance of the proposed control strategy.

6 Proposed control strategy

The general scheme of the proposed control strategy is presented in Fig. 2. The strategy is composed of two types of control modules: one locally implemented on each DG and another one centrally implemented on a microgrid central controller (MGCC). The control equations and detailed explanations about the required communication system are presented in the next subsections. This control structure constitutes the first contribution of this paper. Although some parts of the control modules have been introduced in previous studies, the complete control scheme presented below is new, adequately meets the control objectives described in Section 4, and is relevant for readers interested in control of MGs.

6.1 Local control module

The control implemented on each DG calculates their terms based on local measures and received data from both the central control module and the set N_i of neighbor DGs connected to it through the communication system. It includes a reference generator, an active power regulator and a reactive power regulator.

6.1.1 Reference generator: It builds locally the voltage set-point v_i^* which is used in the internal voltage and current control loops, and in the space-vector pulse width modulator (SVPWM). To ensure the system controllability, a virtual impedance is included in such a way that the output equivalent impedance seen by the DG is dominantly inductive [37, 38]. The voltage set-point is generated as follows

$$v_i^* = V_i \sin(\varphi_i) - Z_v i_i \tag{8}$$

where V_i is the voltage amplitude, φ_i is the phase, Z_v is the virtual impedance and i_i is the output current of the converter.

The amplitude V_i is calculated by adjusting the voltage reference V_0, which is provided by the MGCC, using two correction terms, as follows

$$V_i = V_0 + \delta V_i^Q + \delta V_{PCC}. \tag{9}$$

The first correction term δV_i^Q is provided by the reactive power regulator and the second correction term δV_{PCC} is sent by the voltage control of the MGCC.

In addition, the phase is defined as

$$\varphi_i = \omega_i t + \phi_i + \phi_0 \tag{10}$$

being ω_i the local frequency, ϕ_i the phase provided by the active power regulator, and ϕ_0 the phase-locked loop (PLL) phase provided by the MGCC.

6.1.2 Active and reactive power regulators: The active and reactive power regulators are associated with the control objective (a). These regulators use the powers that come from the neighboring DGs ($P_j\ \forall\ j \in N_i$ for the active power regulator and $Q_j\ \forall\ j \in N_i$

for the reactive power regulator). They are sent over the cooperative communication system (CoCS) in a transmission period T_C. It is also used their respective dispatched references (P_j^D for the active power regulator and Q_j^D for the reactive power regulator), provided by the optimal dispatch of the MGCC and sent over the central communication system (CeCS) in a transmission period T_D. The active power regulator calculates the phase ϕ_i as follows

$$\phi_i = k_{P_i} \int \sum_{j \in N_i} a_{ij} \left(\frac{P_j}{P_j^D} - \frac{P_i}{P_i^D} \right) dt \tag{11}$$

where k_{P_i} is a control parameter.

Similarly, for the reactive power regulator, the correction term δV_i^Q can be calculated as follows,

$$\delta V_i^Q = k_{Q_i} \int \sum_{j \in N_i} a_{ij} \left(\frac{Q_j}{Q_j^D} - \frac{Q_i}{Q_i^D} \right) dt \tag{12}$$

where k_{Q_i} is a control parameter.

Two different transmission periods are associated with these power regulators (i.e., T_C and T_D). This is due to the expected dynamics of the corresponding variables. For instance, local powers need to be updated faster than power references. More details about communications are given in Section 6.3.

6.2 *Central control module*

The central control module is implemented in the MGCC. It sends information to the local control modules using the CeCS. In this module, the optimal dispatch, voltage control and synchronization controller are implemented.

6.2.1 Optimal dispatch: It is associated with the control objective (b). It coordinates the power dispatched by setting the references P_i^D and Q_i^D for each DG, minimizing the generation costs and guaranteeing the power supply.

The power dispatch for a M-nodes MG with N DGs can be determined by solving an AC optimal power flow (OPF) problem [5, 39]. For each time period T_D, it can be modeled as the non-linear optimization problem defined by

$$\min_{P_i^D, Q_i^D, \forall i \in N} \left\{ \sum_{i \in N} f_i(P_i^D) \right\} \tag{13}$$

subject to

$$\mathbf{I_{MG}} = \mathbf{Y_{BUS}} \mathbf{V_{MG}} \tag{14}$$

$$\mathbf{S_{MG}} = 3\, \mathbf{V_{MG}} \circ \mathbf{I_{MG}^*} \tag{15}$$

$$V_{PCC} = V_0 \tag{16}$$

$$P_i^D \leq P_i^{max} \quad \forall\, i \in N \tag{17}$$

$$S_i^D \leq S_i^{max} \quad \forall\, i \in N. \tag{18}$$

In the above formulation, the decision variables correspond to P_i^D and Q_i^D, while $f_i(\cdot)$ represents the generation cost function of the i^{th} DG. The constraint in (14) models the current balance where $\mathbf{I_{MG}} = [\overline{I}_1, ..., \overline{I}_M]^T$ and $\mathbf{V_{MG}} = [\overline{V}_1, ..., \overline{V}_M]^T$ are vectors of the injected currents and nodal voltages, respectively, and $\mathbf{Y_{BUS}} = [\overline{Y}_{ij}^{BUS}] \in C^{M \times M}$ is the admittance matrix of the grid. For modeling purposes, it is desirable to obtain a lower dimensional equivalent of the grid, as it will be discussed later. Then, the current-balance vector must be appropriately labeled in such a way that the first N nodes are those in which the DGs are connected.

Constraint (15) models the powers injection, being $\mathbf{S_{MG}} = [\overline{S}_1, ..., \overline{S}_M]^T$ the vector of the nodal apparent power injected and $\circ$ the Hadamard matrix product operator (i.e, the element-wise multiplication). A linearization procedure can be applied over (15) to obtain a convexified expression with the aim of guarantee the convergence of the optimization problem and reduce the computational time required to solve the optimal dispatch (especially in large scale systems) [40].

Finally, constraint (16) guarantees the compliance of the control objective (c), while constraints (17) and (18) limit the maximum operating values of the powers.

The definition of the problem stated in (13)-(18) requires knowing in advance information about the DGs operation as well as a forecasting estimation of the load consumption. The critical input data is the following:

- *Forecasted load schedule*: accuracy in power dispatch is closely related to load demand. To this end, the programmed load scheduling

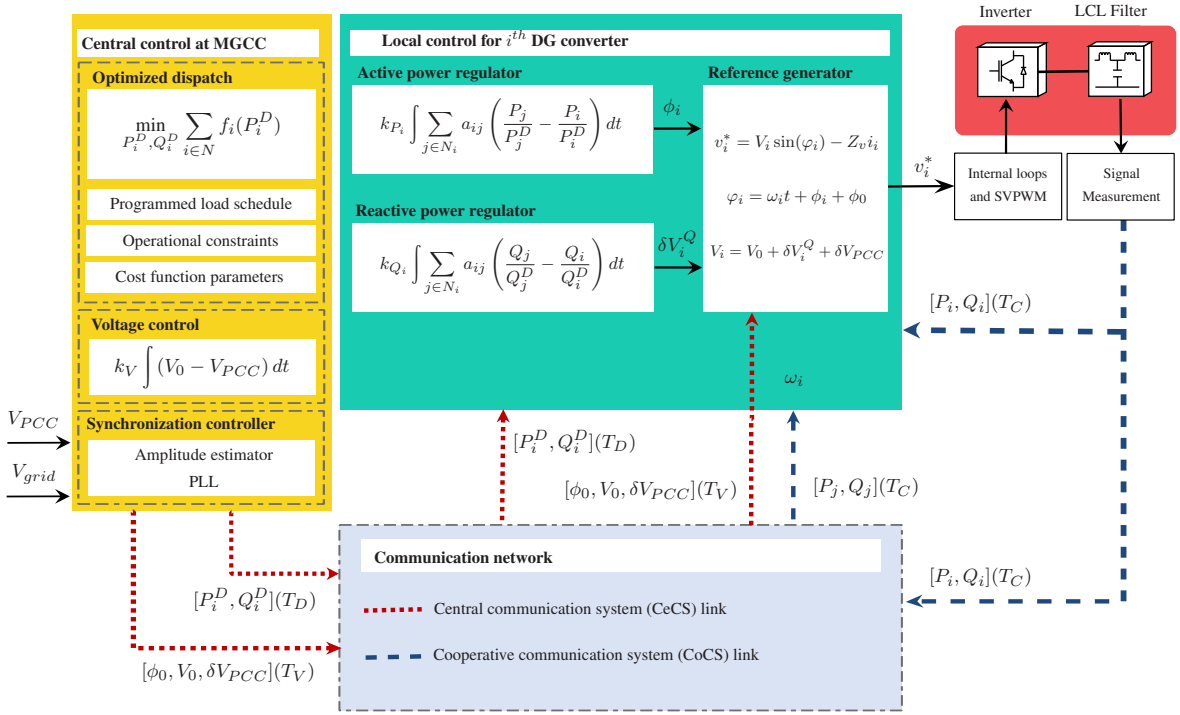

Fig. 2: General scheme of the proposed control.

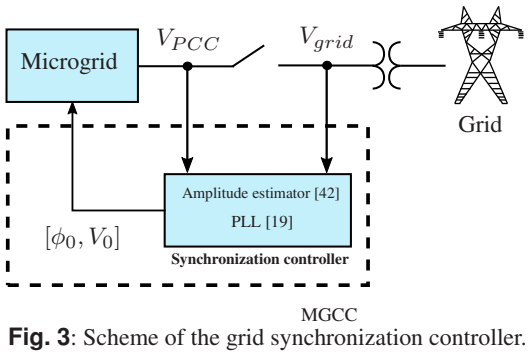

Fig. 3: Scheme of the grid synchronization controller.

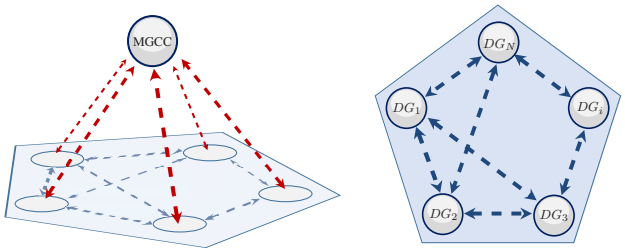

Fig. 4: Communication system schemes: (a) Central communication system (CeCS), (b) Cooperative communication system (CoCS).

can be based on historical consumption profiles or other statistical methods.

- *Operational constraints*: these are based on technical characteristics of the DGs. The aim is to avoid dispatching power values that may overstress the DGs.
- *Cost function parameters*: these are calculated according to the selected cost function model. A common assumption is to approximate the generation cost as a quadratic function of the output active power

$$f_i(P_i^D) = \gamma_i (P_i^D)^2 + \beta_i P_i^D + \alpha_i \quad \forall\, i \in N. \tag{19}$$

Normally, the coefficients γ_i, β_i and α_i are determined according to technical data of the DGs or experimentally testing the MG [41]. The estimation of these coefficients is beyond the scope of this study.

6.2.2 Voltage control: The voltage control is associated with the control objective (c). To this end, the voltage at the PCC is directly sensed by the MGCC. The term δV_{PCC} is calculated as follows

$$\delta V_{PCC} = k_V \int (V_0 - V_{PCC})\, dt \tag{20}$$

where k_V is a control parameter. This term is transmitted to the local modules using the CeCS with a period of T_V.

6.2.3 Grid synchronization controller: In order to allow a smooth transition from islanded mode to grid-connected mode, the MGCC is equipped with a synchronization controller, as it is shown in Fig. 3. It senses the voltages at both sides of the main switch (i.e. V_{PCC} and V_{grid}) in order to ensure that, just before the connection, amplitude and phase of these voltages coincide. An amplitude estimator based on second order generalized integrators [42] is employed to obtain V_0. This amplitude is used in the MGCC for the centralized PCC voltage control and is also sent (using the CeCS with a period of T_V) to all DGs to compute their local voltage references. A centralized phase-locked loop (PLL), based on the synchronous reference frame cross product [19], is used to calculate the phase shift ϕ_0 necessary to synchronize both sides of the switch. This phase shift is also sent using the CeCs with a period of T_V to all DGs and used locally to compute local references.

6.3 Communication framework

The communication network supports the data exchange between DGs for control and monitoring purposes. The proposed control acts over a dual communication system which uses a central (one-to-all) and a cooperative (one-to-neighbors) scheme. Each communication system has its transmission time period (i.e, T_V and T_D for the central system and T_C for the cooperative system).

6.3.1 Central communication system (CeCS): In this communication system, the MGCC is considered as the central unit of a one-to-all scheme, as it is shown in Fig. 4(a). The central control module terms are transmitted in two different time periods, being $T_D >> T_V$. The main reason for implementing two transmission periods is the difference in the dynamics of the variables. Particularly, the dispatch terms are updated in real-time but at a lower transmission frequency than the voltage control correction term.

6.3.2 Cooperative communication system (CoCS): In this communication system, the DGs are connected in a sparse network (one-to-neighbors scheme) which does not require a central controller, as it is shown in Fig. 4(b). The CoCS can be described using a graph defined as $\mathcal{G} = (N, \mathcal{E}, \mathbf{A})$, where $N = \{1, ..., N\}$ is the set of nodes with DG units, and $\mathcal{E} \subseteq N \times N$ is the set of edges that represents the communication links. The elements a_{ij} form the adjacency matrix $\mathbf{A} \in R^{N \times N}$ such that $a_{ij} = a_{ji} = 1$ if there is a communication link (edge) between the unit i and the unit j, and $a_{ij} = a_{ji} = 0$ otherwise. Also, the degree matrix is expressed as $\mathbf{D} = \text{diag}\{d_i\}$, where $d_i = \sum_{j \in N_i} a_{ij}$, and the Laplacian matrix is defined as $\mathbf{L} = \mathbf{D} - \mathbf{A}$. This matrix will be used for the modeling and stability analysis of the control strategy. It is assumed a bidirected communication graph $\mathcal{G}$ where at least it exists a direct path through the communication links between any distinct pair of units.

7 System modeling

In this section, the system modeling is presented. The proposed closed-loop small-signal approach constitutes the second contribution of this paper. This modeling is used in the next Section to set the control parameters and guarantee the system stability.

7.1 Microgrid plant modeling

As a starting point, the microgrid plant modeling is derived. For this purpose, the admittance matrix of the grid $\mathbf{Y_{BUS}}$ can be rewritten using Kron's reduction as $\mathbf{Y_{BUS}^K} = [\overline{Y}_{ij}] \in C^{N \times N}$ [43–45]. The use of this technique allows to reduce the size of the matrix, compacting the information of the entire MG in the N nodes in which DGs are connected. The equivalent reduced current balance can be formulated as

$$\mathbf{I} = \mathbf{Y_{BUS}^K V} \tag{21}$$

where $\mathbf{I} = [\overline{I}_1, ..., \overline{I}_N]^T$ and $\mathbf{V} = [\overline{V}_1, ..., \overline{V}_N]^T$. Using power flow analysis, the active and reactive powers delivered by each source can be derived as

$$P_i = 3V_i \sum_{j=1}^{N} V_j Y_{ij} \cos(\delta_i - \delta_j - \theta_{ij}) \tag{22}$$

$$Q_i = 3V_i \sum_{j=1}^{N} V_j Y_{ij} \sin(\delta_i - \delta_j - \theta_{ij}) \tag{23}$$

where V_i and δ_i are the magnitude and angle of the phasor $\overline{V}_i$, and Y_{ij} and θ_{ij} are the magnitude and angle of $\overline{Y}_{ij}$. From (22) and (23), a small-signal representation is obtained as follows

$$P_i \cong P_i^q + \widehat{P}_i = P_i^q + \sum_{j=1}^{N} \frac{\partial P_i}{\partial V_j}\widehat{V}_j + \sum_{j=1}^{N} \frac{\partial P_i}{\partial \delta_j}\widehat{\delta}_j \quad (24)$$

$$Q_i \cong Q_i^q + \widehat{Q}_i = Q_i^q + \sum_{j=1}^{N} \frac{\partial Q_i}{\partial V_j}\widehat{V}_j + \sum_{j=1}^{N} \frac{\partial Q_i}{\partial \delta_j}\widehat{\delta}_j \quad (25)$$

where P_i^q and Q_i^q are the quiescent components, and $\widehat{P}_i$ and $\widehat{Q}_i$ are the small-signal perturbations of the active and reactive powers, respectively. In order to analyze the small-signal behaviour, a matrix arrangement can be obtained as follows

$$\widehat{\mathbf{P}} = \mathbf{G_V^P}\widehat{\mathbf{V}} + \mathbf{G_\delta^P}\widehat{\boldsymbol{\delta}} \quad (26)$$

$$\widehat{\mathbf{Q}} = \mathbf{G_V^Q}\widehat{\mathbf{V}} + \mathbf{G_\delta^Q}\widehat{\boldsymbol{\delta}} \quad (27)$$

being $\widehat{\mathbf{P}} = [\widehat{P}_1, ..., \widehat{P}_N]^T$, $\widehat{\mathbf{Q}} = [\widehat{Q}_1, ..., \widehat{Q}_N]^T$, $\widehat{\mathbf{V}} = [\widehat{V}_1, ..., \widehat{V}_N]^T$ and $\widehat{\boldsymbol{\delta}} = [\widehat{\delta}_1, ..., \widehat{\delta}_N]^T$ column vectors of the small-signal portions of active powers, reactive powers, voltage magnitudes and phases, respectively, and $\mathbf{G_V^P} = [\frac{\partial P_i}{\partial V_j}]$, $\mathbf{G_\delta^P} = [\frac{\partial P_i}{\partial \delta_j}]$, $\mathbf{G_V^Q} = [\frac{\partial Q_i}{\partial V_j}]$ and $\mathbf{G_\delta^Q} = [\frac{\partial Q_i}{\partial \delta_j}]$ are matrices in $R^{N\times N}$.

Considering that the virtual impedance is included in the internal control loops, a predominantly inductive output equivalent impedance is obtained and thus it is possible to assume that $\mathbf{G_V^P} \cong 0$ and $\mathbf{G_\delta^Q} \cong 0$ in (26) and (27), obtaining a more compact MG plant modeling [33, 45]

$$\widehat{\mathbf{P}} = \mathbf{G_\delta^P}\widehat{\boldsymbol{\delta}} \quad (28)$$

$$\widehat{\mathbf{Q}} = \mathbf{G_V^Q}\widehat{\mathbf{V}}. \quad (29)$$

7.2 Control modeling

Next, the modeling of the control strategy is presented. Active and reactive power regulators and voltage control are described in the next subsections.

7.2.1 Active and reactive power regulators: The equation of the active power regulator (11), can be expressed for each DG in a frequency-domain small-signal representation as

$$\widehat{\phi}_i = \frac{k_{P_i}}{s}\sum_{j\in N_i} a_{ij}\left(\frac{\widehat{P}_j}{P_j^D} - \frac{\widehat{P}_i}{P_i^D}\right). \quad (30)$$

Considering the definition of the Laplacian matrix $\mathbf{L}$, the N active power regulator equations (30) can be arranged in a matrix representation as

$$\widehat{\boldsymbol{\phi}} = -\frac{\mathbf{k_P}}{s}\mathbf{L}(\mathbf{P^D})^{-1}\widehat{\mathbf{P}} = \mathbf{H_P^\phi}\widehat{\mathbf{P}} \quad (31)$$

where $\mathbf{k_P} = \text{diag}\{k_{P_i}\}$ and $\mathbf{P^D} = \text{diag}\{P_i^D\}$ are diagonal matrices, and $\widehat{\boldsymbol{\phi}} = [\widehat{\phi}_1, ..., \widehat{\phi}_N]^T$ is a column vector of the small-signal phases.

Similarly, the reactive power regulator (12) can be expressed for each DG in a frequency-domain small-signal representation as

$$\widehat{\delta V}_i^Q = \frac{k_{Q_i}}{s}\sum_{j\in N_i} a_{ij}\left(\frac{\widehat{Q}_j}{Q_j^D} - \frac{\widehat{Q}_i}{Q_i^D}\right) \quad (32)$$

which can be arranged in a matrix representation as

$$\widehat{\boldsymbol{\Delta}}_{\boldsymbol{Q}} = -\frac{\mathbf{k_Q}}{s}\mathbf{L}(\mathbf{Q^D})^{-1}\widehat{\mathbf{Q}} = \mathbf{H_Q^\Delta}\widehat{\mathbf{Q}} \quad (33)$$

where $\mathbf{k_Q} = \text{diag}\{k_{Q_i}\}$ and $\mathbf{Q^D} = \text{diag}\{Q_i^D\}$ are diagonal matrices, and $\widehat{\boldsymbol{\Delta}}_{\boldsymbol{Q}} = [\widehat{\delta V}_1^Q, ..., \widehat{\delta V}_N^Q]^T$ is a column vector of the small-signal voltage correction terms.

Expressions (31) and (33) allow to relate the active and reactive powers injected by each DG with the power regulation terms. In each expressions, a transfer function term is proposed (i.e, $\mathbf{H_P^\phi}$ and $\mathbf{H_Q^\Delta}$, respectively) in order to compact the notation.

7.2.2 Voltage control: The steps for the derivation of the voltage control transfer function are explained below. As a starting point, the voltage equation in (9) is expressed equivalently in a frequency-domain small-signal representation as

$$\widehat{\mathbf{V}} = \widehat{\boldsymbol{\Delta}}_{\boldsymbol{Q}} + \widehat{\boldsymbol{\Delta}}_{\mathbf{PCC}}. \quad (34)$$

The first term, $\widehat{\boldsymbol{\Delta}}_{\boldsymbol{Q}}$, was previously obtained in (33), while the second term corresponds to the matrix that arrange the PCC voltage control term that is applied in each local control.

Note that, unlike other variables, the PCC voltage control is implemented over a single node of the MG. It is expected that the PCC is located at one node in which no DGs are connected, therefore, a node that is not included in the reduced admittance matrix $\mathbf{Y_{BUS}^K}$. For this reason, it is required to find an expression that relates the vector of voltages $\mathbf{V}$ with the voltage at the PCC. The MG current balance in (14) can be expressed as

$$\mathbf{I_{MG}} = \begin{bmatrix}\mathbf{I}\\ \mathbf{I_{NG}}\end{bmatrix} = \begin{bmatrix}\mathbf{A} & \mathbf{B}\\ \mathbf{C} & \mathbf{D}\end{bmatrix}\begin{bmatrix}\mathbf{V}\\ \mathbf{V_{NG}}\end{bmatrix} = \mathbf{Y_{BUS}V_{MG}} \quad (35)$$

where $\mathbf{I_{NG}} = [\overline{I}_{N+1}, ..., \overline{I}_M]^T$ and $\mathbf{V_{NG}} = [\overline{V}_{N+1}, ..., \overline{V}_M]^T$ are the current and voltage vectors at the nodes in which there are no DGs connected. For this reason, its corresponding injected currents are equal to zero, which is the principle of Kron's reduction [43, 44]. Thus,

$$\begin{bmatrix}\mathbf{I}\\ 0\end{bmatrix} = \begin{bmatrix}\mathbf{A} & \mathbf{B}\\ \mathbf{C} & \mathbf{D}\end{bmatrix}\begin{bmatrix}\mathbf{V}\\ \mathbf{V_{NG}}\end{bmatrix} \quad (36)$$

which allows to obtain

$$\mathbf{V_{NG}} = -\mathbf{D}^{-1}\mathbf{C}\mathbf{V}. \quad (37)$$

Then, a selector row vector with all the elements equal to 0 except a 1 located at the position corresponding to the PCC node according to the labeling, $\mathbf{R} = [0, ..., 1, ..., 0]$ of size $1 \times (M - N)$ can be included to obtain the voltage V_{PCC} as a function of $\mathbf{V}$

$$V_{PCC} = -\mathbf{R}\mathbf{D}^{-1}\mathbf{C}\mathbf{V} = \mathbf{H_V^\Delta}\mathbf{V} \quad (38)$$

which can be expressed as the transfer function $\mathbf{H_V^\Delta}$.

Once obtained the expression of V_{PCC} in (38), a small-signal representation can be derived as

$$V_{PCC} \cong {V_{PCC}}^q + \sum_{j=1}^{N}\frac{\partial V_{PCC}}{\partial V_j}\widehat{V}_j + \sum_{j=1}^{N}\frac{\partial V_{PCC}}{\partial \delta_j}\widehat{\delta}_j \quad (39)$$

and a small-signal matrix arrangement can be obtained as

$$\widehat{\mathbf{V}}_{\mathbf{PCC}} = \mathbf{G_V^{PCC}}\widehat{\mathbf{V}} + \mathbf{G_\delta^{PCC}}\widehat{\boldsymbol{\delta}} \quad (40)$$

where $\mathbf{G_V^{PCC}} = [\frac{\partial V_{PCC}}{\partial V_j}]$ and $\mathbf{G_\delta^{PCC}} = [\frac{\partial V_{PCC}}{\partial \delta_j}]$ are vectors in $R^{1\times N}$.

The next step is to obtain a frequency-domain small-signal representation of the voltage control in (20). It can be expressed as

$$\widehat{\delta V}_{PCC} = -\frac{k_V}{s}\widehat{V}_{PCC}. \tag{41}$$

Notice that (41) corresponds to the PCC voltage control term that is calculated at the MGCC and send to each local controller. For this reason, to adequately add it on the matrix representation, it is necessary to reply the term using $\mathbf{H_{ones}}$ a column vector of $N \times 1$ with all the elements equal to 1. Thus, it is obtained

$$\widehat{\mathbf{\Delta}}_{\boldsymbol{PCC}} = -\frac{\mathbf{k_V}}{s}\mathbf{H_{ones}}\widehat{\mathbf{V}}_{\mathbf{PCC}}. \tag{42}$$

where $\mathbf{k_V} = \text{diag}\{k_V\}$.

Finally, inserting (40) in (42) it is possible to obtain

$$\widehat{\mathbf{\Delta}}_{\boldsymbol{PCC}} = \mathbf{H}_{\mathbf{V}}^{\mathbf{PCC}}\widehat{\mathbf{V}} + \mathbf{H}_{\boldsymbol{\delta}}^{\mathbf{PCC}}\widehat{\boldsymbol{\delta}} \tag{43}$$

which properly relates the small-signal variables (including the second term in the right side of equation (34), $\widehat{\mathbf{\Delta}}_{\boldsymbol{PCC}}$). Therefore, an useful transfer function representation for closed-loop small-signal modeling has been derived in (43), as it can be seen in next Section.

7.3 *Closed-loop small-signal models*

The modeling equations previously presented are the base for the closed-loop small-signal modeling formulation. Note that previous approaches based on droop-free schemes fail at providing such closed-loop models [33, 34].

On the one hand, regarding the voltage-reactive power loop, using the plant modeling in (29), the control equation (33), and inserting (43) in (34), it is possible to obtain the closed-loop scheme shown in Fig. 5. On the other hand, regarding the frequency-active power loop, notice that a small-signal equation is missing to relate the plant modeling (28) and the control equation (31). To derive an expression of the small-signal perturbation of the frequency, consider the generation of the voltage set-point in (8), where each v_i^* is locally built. If all the local voltages are referred to a common framework ω_0 (i.e., the nominal frequency), the set-points can be reformulated as

$$v_i^* = V_i \sin(\omega_0 t + \delta_i) - Z_v i_i \tag{44}$$

with $\delta_i = (\omega_i - \omega_0)t + \phi_i + \phi_0$. This means that the phase of the voltage phasor δ_i is transiently affected by the variation of the local frequency with respect to the nominal frequency. These variations on the local frequencies are necessary to give the correct dynamics to the operation of the DGs and, therefore, to achieve the desired steady-state values in accordance with the control objectives. By expressing δ_i in small-signal

$$\widehat{\delta}_i = \widehat{\omega}_i t + \widehat{\phi}_i \tag{45}$$

a matrix representation can be obtained as

$$\widehat{\boldsymbol{\delta}} = \widehat{\boldsymbol{\omega}} t + \widehat{\boldsymbol{\phi}}. \tag{46}$$

where $\widehat{\boldsymbol{\omega}} = [\widehat{\omega}_1, ..., \widehat{\omega}_N]^T$. With this expression, the small-signal model of the frequency-active power loop is closed and can be represented as it is shown in Fig. 6.

It is worth mentioning that a connection between variables $\widehat{\delta}_i$ and $\widehat{\phi}_i$ is not previously presented in droop-free control schemes [33, 34] and, therefore, the model shown in Fig. 6 is a contribution of this paper. This model is essential to design the control parameters, as it is shown below.

8 Control parameters design

As starting point, the closed-loop small-signal modeling derived in the previous Section is used to determine the location of the system poles. The parameters can be grouped according to the two closed-loop models: the set k_{P_i} is associated with the frequency-active power loop while the set k_{Q_i} and k_V with the voltage-reactive

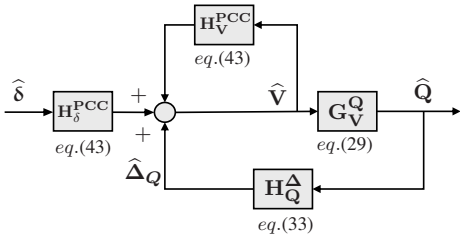

Fig. 5: Diagram of the voltage-reactive power small-signal model.

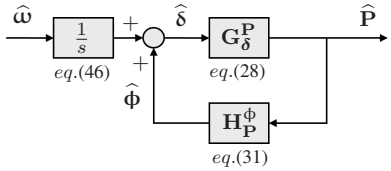

Fig. 6: Diagram of the frequency-active power small-signal model.

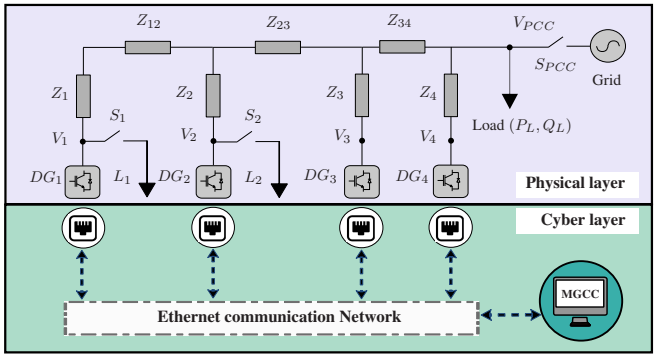

Fig. 7: Diagram of the laboratory microgrid setup.

power loop. For the sake of simplicity, all the elements of k_{P_i} and k_{Q_i} are selected as the single values k_P and k_Q, leading to a homogeneous network and simplifying the analysis in a possible changing environment.

To guarantee the stability of the system in all operating scenarios it is recommended to design the values of the control parameters for a nominal case scenario (assuming that each DG delivers their nominal power) and then analyze the boundary scenarios (for instance, when the DGs deliver their maximum capacity) using advanced stability methods such as Lyapunov stability criteria [46]. To calculate the quiescent values and the dispatch references, it is necessary to solve the MG power flow. Also, the Laplacian matrix $\mathbf{L}$ should be determined as discussed in previous sections. Once these values are defined, the impact on the poles of the closed-loop model produced by the control parameters can be analyzed as indicated below.

The laboratory microgrid used for the experimental test follows the schematic topology shown in Fig. 7 (more details about its technical characteristics are given in the next Section). For the closed-loop plots, the parameters listed in Table 2 and 3 were considered.

The design of k_P focuses on selecting an appropriate value in order to ensure stability while the dominant pole should be located to avoid undesired oscillations. Fig. 8(a) shows the dominant closed-loop poles for $0.01 \leq k_P \leq 0.5$. Notice that the increase in the value of k_P moves the dominant single pole (in red) over the x-axis to the left. For values close to k_P = 0.5, the closest pair of conjugated poles (in green) interact with the real single pole. A value of k_P = 0.1 rad/s was chosen for the experimental tests to avoid this undesired interaction.

Since k_Q and k_V are associated with the voltage-reactive power loop, it is possible to set one parameter to analyze the closed-loop poles with respect to the other. Fig. 8(b) presents the dominant closed-loop poles for k_Q = 1 V/s and $0.01 \leq k_V \leq 0.5$. The increase in the value of k_V moves the dominant poles to the right. Therefore, to avoid risking the relative stability of the system, a value of k_V = 0.3 s^{-1} was chosen. Finally, the stability was proved for the

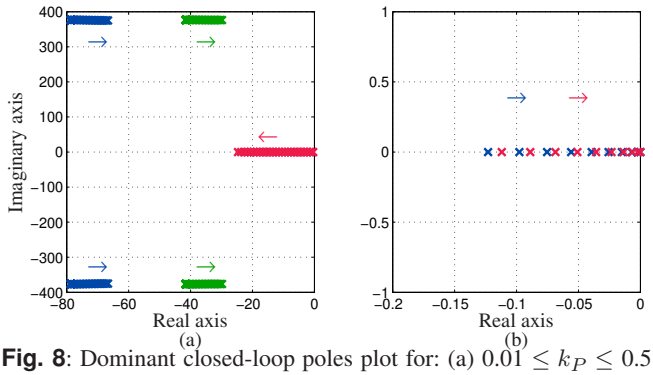

Fig. 8: Dominant closed-loop poles plot for: (a) $0.01 \leq k_P \leq 0.5$ and (b) $0.01 \leq k_V \leq 0.5$ with $k_Q = 1$.

selected control parameters using Lyapunov criteria (lineal matrix inequality based analysis [47]). For this, boundary scenarios were evaluated concluding that these parameters fulfill the Lyapunov conditions and thus, guarantee the stability for all expected operating scenarios as well as the changes that these can produce over the plant.

Table 2 Control parameters

Parameter	Symbol	Quantity
Nominal frequency	ω_N	120π rad/s
Nominal voltage	V_N	110 V rms
Virtual impedance	Z_v	3.77 Ω
Active power control parameter	k_P	0.1 rad/s
Reactive power control parameter	k_Q	1 V/s
Voltage control parameter	k_V	0.3 s^{-1}
Local transmission period	T_C	0.05 s
Voltage transmission period	T_V	0.1 s
Dispatch transmission period	T_D	5 s

Table 3 Parameters of the experimental microgrid setup

Parameter	Symbol	Quantity
Microgrid nominal power	S	5 kVA
Line impedance 1	Z_1	0.50+0.376j Ω
Line impedance 2	Z_2	0.50+0.376j Ω
Line impedance 3	Z_3	1.13+0.226j Ω
Line impedance 4	Z_4	1.13+0.226j Ω
Line impedance 12	Z_{12}	0.754j Ω
Line impedance 23	Z_{23}	0.376j Ω
Line impedance 34	Z_{34}	0.376j Ω
Main load	Load (P_L, Q_L)	Programmable

Table 4 Loads for the experimental test

OP	OP1	OP2	OP3	OP4
P_L	1100 W	1500 W	1100 W	1500 W
Q_L	0 VAr	0 VAr	200 VAr	400 VAr
Dispatch scenario	I	I	II	II
Time interval	0 $\leq$t<20 s	20 $\leq$t<40 s	40 $\leq$t<60 s	60 $\leq$t< 100 s

Table 5 Cost function parameters selected for the experimental test

Parameter	Quantity	Parameter	Quantity	Parameter	Quantity
γ_1, γ_2	0.150 W^{-2}	β_1, β_2	0.100 W^{-1}	α_1, α_2	0
γ_3	0.075 W^{-2}	β_3	0.050 W^{-1}	α_3	0

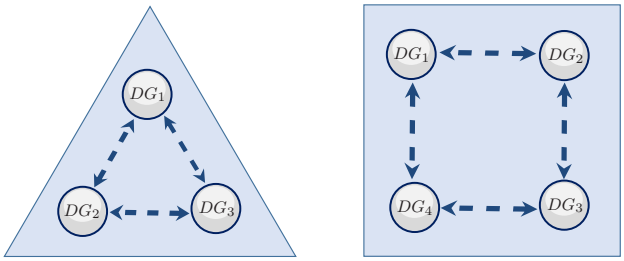

Fig. 9: Cooperative communication system (CoCS) implemented for: (a) Test 1 and 2, (b) Test 3.

9 Experimental results

This Section presents selected experimental results that validate the features of the proposed control. First, the laboratory microgrid setup is described. Next, the design of the test case is discussed. Finally, the experimental results are presented analyzing the evaluation of the performance metrics.

9.1 Laboratory microgrid setup

A three-phase microgrid was implemented to carry out the experimental tests. The laboratory setup was built following the topology shown in Fig. 7. The MG is composed of four generation nodes DG_i, a voltage power source that emulates the main grid, a programmable load, two local load L_i connected through the switches S_i and distribution lines emulated using resistors and inductors with the values listed in Table 3. Each generation node consists of a three-phase IGBT full-bridge power inverter fed by an AMREL DC source, a damped LCL output filter and a control platform implemented on a Texas Instruments DSP. The cyber layer is composed of a dedicated Ethernet network running over a User Datagram Protocol/Internet Protocol (UDP/IP) configured according to the characteristics discussed in Section 6.3. More detailed information about sensing and communication stages of this laboratory microgrid can be found in [48].

The optimal dispatch is obtained using a real-time approach. The updated load schedule and the data discussed in Section 6 is gathered by the MGCC, where the optimization algorithm implemented in AMPL and solved with IPOPT is executed [49, 50]. In all the tests, a workstation with an Intel i7-4749 processor and 16 GB RAM was used.

9.2 Design of test cases

In this subsection, the discussion related to the design of the experimental test cases is presented. The design of the experiments must be done specially considering the control objectives defined in Section 4, since the evaluation performance metrics (Section 5) were formulated based on them. Thus, the test cases must include at least:

- An experimental test in which the main load is programmed in different operating points (i.e., different values of active and reactive power consumption) in order to evaluate the dispatch performance and the power sharing capability of the control strategy.
- An experimental test in which the variations of the MG load affect the voltage profile and the PCC is regulated by the voltage controller.
- An experimental test in which the grid synchronization controller operates in order to connect the MG to the main grid without relevant high power overshoots and undesired current and voltage peaks.

Furthermore, to complement the performance evaluation of the control strategy under realistic and adverse scenarios, the following aspects are going to be included:

- An experimental test in which the performance of the control strategy is evaluated in the presence of renewable generation (intermittent power sources).

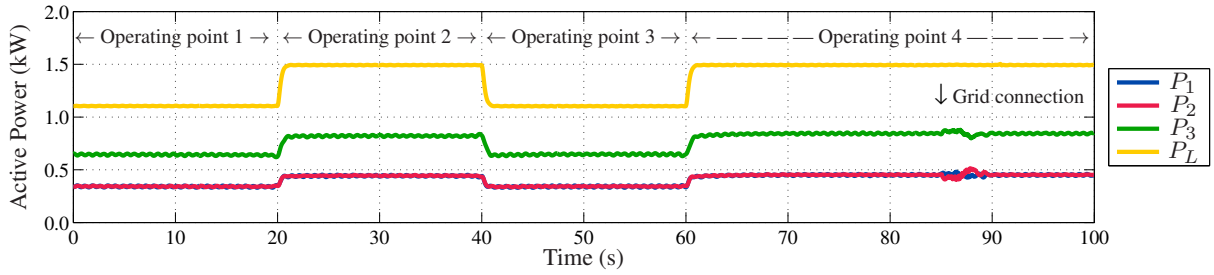

Fig. 10: Test case 1: active powers of the load and the DGs.

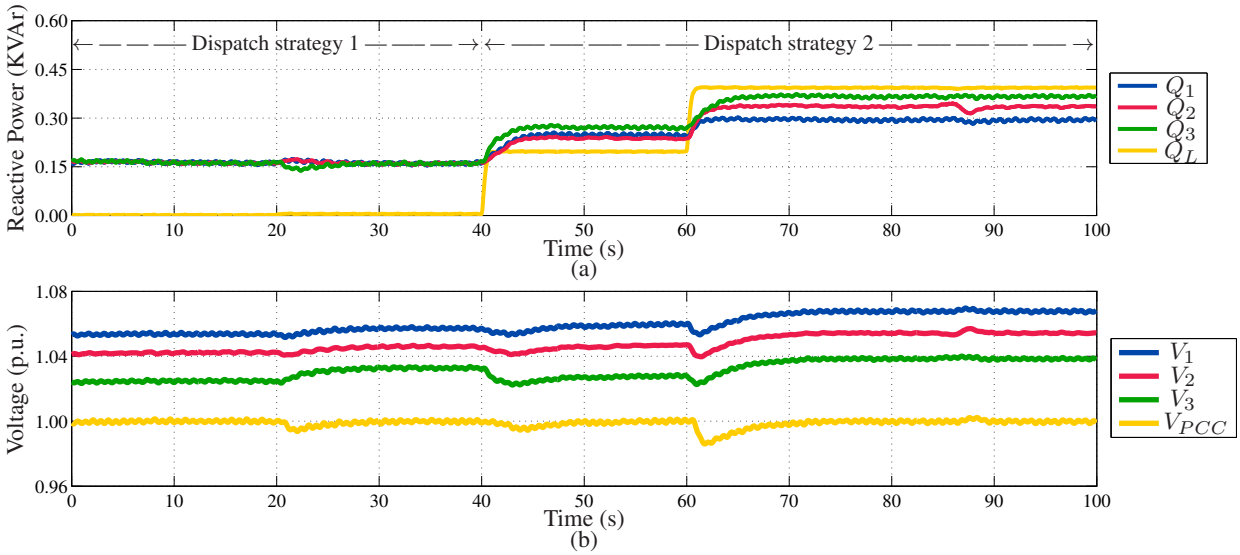

Fig. 11: Test case 1: (a) reactive powers of the load and the DGs and (b) voltages of the PCC and the DGs.

• An experimental test in which the transmission periods are magnified, to evaluate the impact of the data transmission/reception features over the strategy performance.
• An experimental test in which the control strategy operates under adverse communications features, such as data reception delays.
• An experimental test in which the MGCC fails during a time interval.

It is worth noting that the characteristic of the control objectives addressed in the proposal allows to analyze the strategy performance in a segregate way, i.e., emulating contingencies separately according to the variables and time of responses. The design of experimental test cases with simultaneous events does not provide new or relevant information to the evaluation stage and for this reason, the test cases are designed considering single event scenarios.

Based on the aspects presented above, three experimental test cases were considered:

• Test case 1: In this test a general performance evaluation test is considered. Different power operating points are tested by varying the programmable main load. Also, a grid connection is executed.
• Test case 2: In this test, one of the DGs is operated as intermittent source while a MGCC failure is induced.
• Test case 3: In this test, the transmission periods of the communication systems are magnified while data reception delays are induced.

As discussed in Section 1, it was not possible to find in the specialized literature similar control strategies (based on principles different from those of standard droop control) capable of simultaneously guaranteeing the control objectives covered in this proposal (see Table 1). For this reason, no other strategies will be used as benchmark for the control performance evaluation, which will be based on the proposed metrics and the different test scenarios.

9.3 Test case 1: Performance evaluation test

The first test was developed with the aim of evaluating the performance of the control strategy. The first three DGs were considered (i.e., DG_1, DG_2 and DG_3) while the fourth DG (DG_4) remained disconnected during the test. The CoCS was implemented considering the scheme depicted in Fig. 9(a). Regarding the loads, the main load was programmed to simulate four different operating point (OPs), with the values of the active and reactive powers (P_L, Q_L) for the time intervals presented in Table 4. During this test, switches S_1 and S_2 remained open, thus L_1 and L_2 were disconnected. During the operation in OP4, S_{PCC} was closed at $t = 85$ s to emulate the transition from islanded mode to grid-connected mode.

The dispatch operation related to the reactive powers was divided into two scenarios. The dispatch scenario I was implemented while

Table 6 Powers of the optimal dispatch

OP	P_1^D	P_2^D	P_3^D	Q_1^D	Q_2^D	Q_3^D
1	323.26	323.26	605.12	100	100	100
2	432.91	432.93	795.71	100	100	100
3	323.72	323.73	608.41	197.88	191.35	213.10
4	435.49	435.71	808.11	246.51	281.34	314.05

Table 7 Performance metrics of the power-sharing, power dispatch and PCC voltage regulation for the experimental test

OP	e^{PS}	e^{QS}	e^{PD}	e^{QD}	e^{V}
1	0.15%	0%	2.62%	-	0%
2	0.12%	0%	1.94%	-	0.20%
3	0.35%	1.85%	2.56%	2.27%	0%
4	0.29%	1.15%	2.18%	2.01%	0.20%

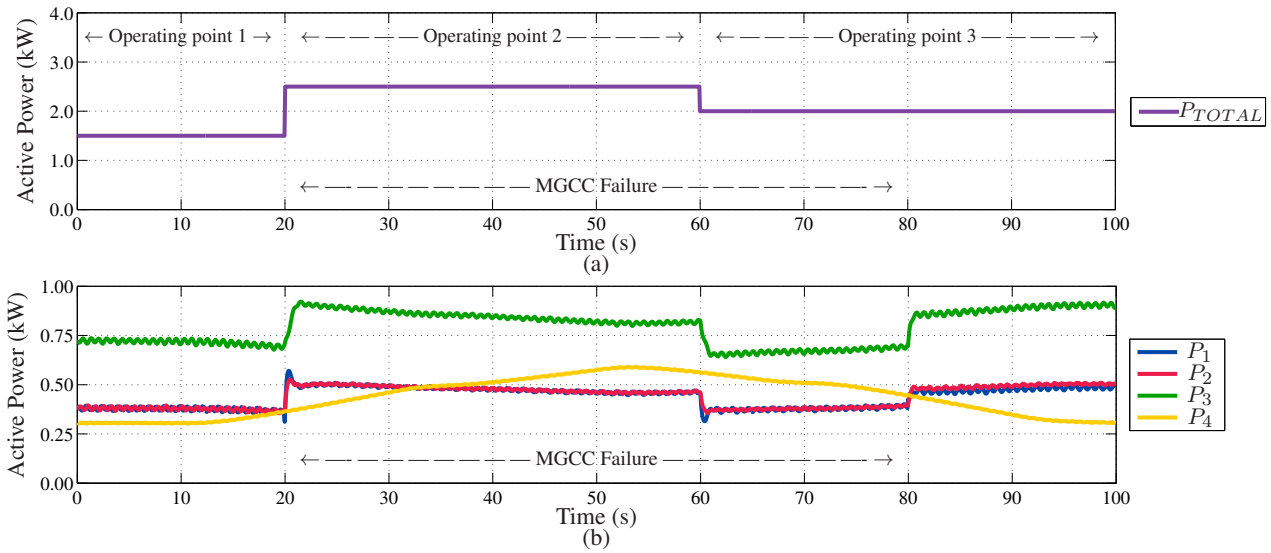

Fig. 12: Test case 2: (a) active power of the load and (b) active powers of the DGs.

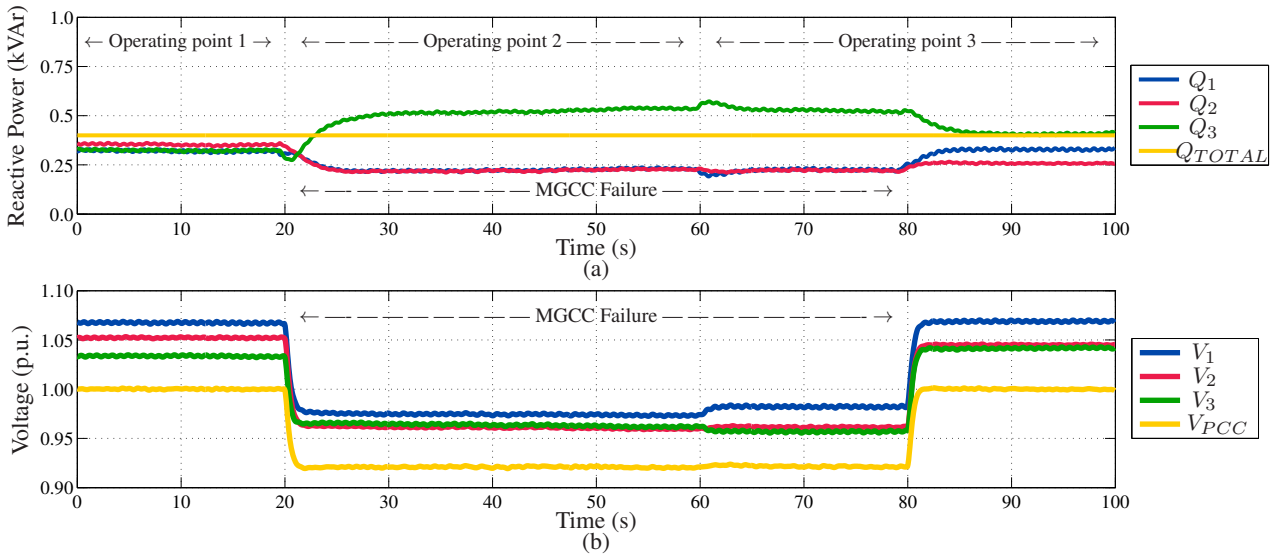

Fig. 13: Test case 2: (a) reactive powers of the load and the DGs and (b) voltages of the PCC and the DGs.

$Q_L = 0$ VAr (i.e., during OP1 and OP2). On it, the references Q_i^D were set in a base value of 100 VAr for all the DGs. In this scenario it is expected an equal reactive power injection on each DG. In the dispatch scenario II, implemented while $Q_L \neq 0$ (i.e., during OP3 and OP4), the reactive powers were selected as decision variables of the dispatch problem and calculated according to the problem formulation previously presented.

The cost function parameters selected for the experimental test are listed in Table 5. For each OP, the optimal dispatch power references are presented in Table 6. The experimental results are shown in Fig. 10 and 11, and Table 7.

Regarding the control objective (a), Fig. 10 shows the active powers P_i of the DGs, and the load P_L, while Fig. 11(a) shows the reactive powers Q_i of the DGs, and the load Q_L. In both figures, fast dynamic responses to the load changes are observed with acceptable slight ripples and overshoots.

Table 7 lists the performance metrics defined in Section 5, which permits to assess the accuracy of the control proposal in practice. The maximum errors for each OP are presented. The dispatch scenarios have a clear impact over the reactive power sharing. During the dispatch scenario I, the reactive powers injected by each DG are equal, corresponding to a dispatch error of 0%. Next, during the dispatch scenario II, the dispatched references lead to differences between the injected reactive powers that correspond to small dispatch errors. Hence, it can be concluded that for different dispatching scenarios, an accurate power-sharing is achieved. Note that the measured errors are all below 2%.

Regarding control objective (b), it is important to highlight that, considering the characteristics of the optimization problem and the convexification approach, the optimal power dispatch is always achieved. In Table 7, the dispatch errors calculated according to (6) are presented. Reactive power errors for the dispatch scenario I are omitted since its calculation is meaningless, considering that in this scenario the reactive power references were set to constant values to evaluate the power equalization capability of the control scheme. Notice that all the errors present values below 3%, which are negligible in a real scenario.

Regarding control objective (c), Fig. 11(b) shows the voltages at the terminals of the DGs, V_i, and the PCC, V_{PCC}. The changes produced by the OPs allow observing how the control acts over the MG voltage profile with a fast recovery in each load change. Note that V_{PCC} practically reaches a value of 1 p.u. in all the OPs, with a maximum error of 0.2% as it is shown in Table 7.

At $t = 85$ s the PCC switch S_{PCC} was closed and the MG was connected to the grid. To this end, a PLL was implemented to synchronize the phase of V_{PCC} with the grid voltage before the connection, as explained in Section 6.2. After the connection of the grid a perturbation is presented with a duration of approximately 4

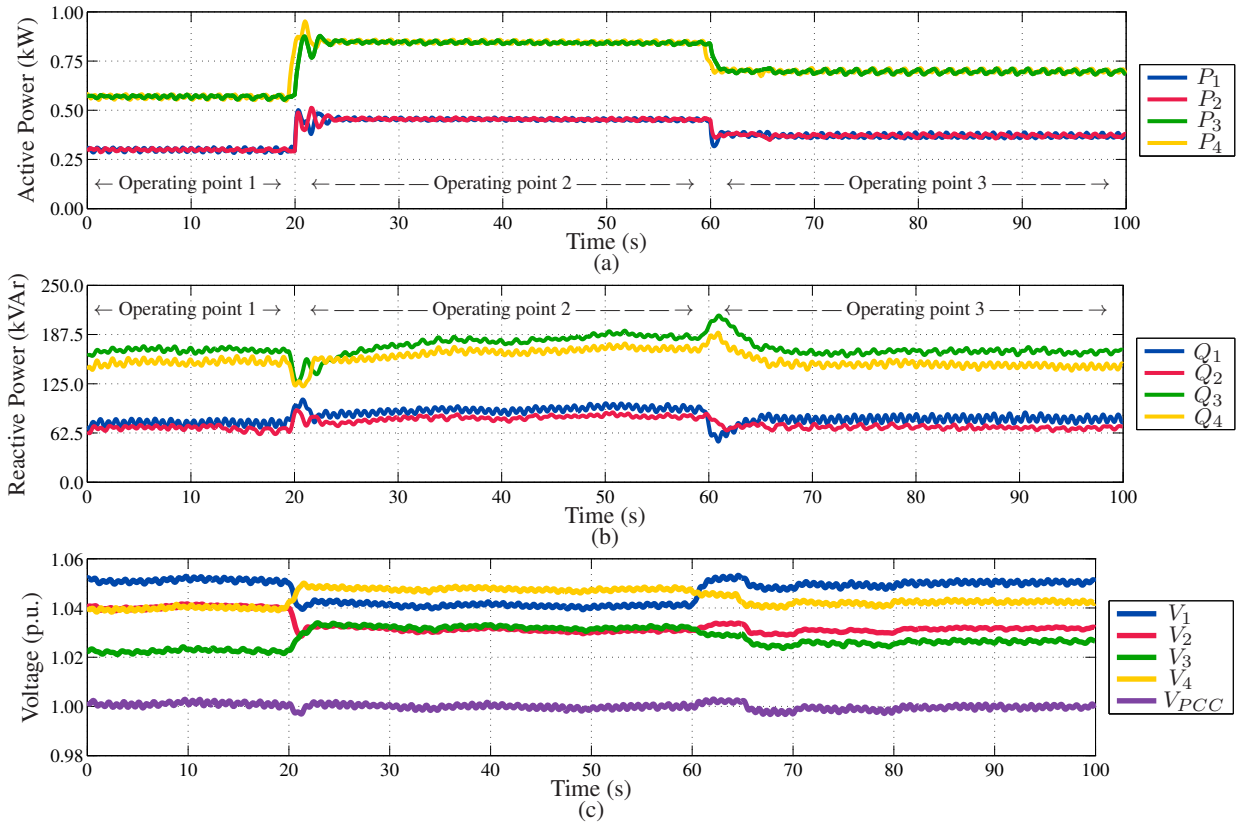

Fig. 14: Test case 3: (a) active powers, (b) reactive powers, and (c) voltages.

s. Since no significant power overshoots are observed, the transition can be considered smooth and without relevant impacts over the MG operation.

9.4 Test case 2: Renewable generation and MGCC failure test

The second test was developed in order to evaluate the performance of the control strategy in the presence of a renewable DG and a MGCC temporary failure. The first three DGs were implemented as controllable DGs (considering a CoCS as depicted in Fig. 9(a)) while the fourth DG operates as an intermittent renewable power source.

Regarding the MG loads, during this test a load profile was built using the main load and the local loads L_1 and L_2 with the values and time intervals indicated in Table 8. P_{TOTAL} represents the total active power of the loads (i.e., P_L together with the corresponding local loads connected during the OP) and Q_{TOTAL} represents the total reactive power (equal to Q_L considering that the local loads are purely resistive).

A MGCC failure scenario was implemented from t = 20 s to t = 80 s. During this interval, the MGCC data transmission was disabled and no data was sent through the CeCS. Regarding the dispatch, the same cost function parameters selected for the previous test were implemented (see Table 5).

The experimental results are presented in Fig. 12 and Fig. 13. In Fig. 12(a) the profile of the total active power of the loads P_{TOTAL} is shown, while the active powers of the DGs are depicted in Fig. 12(b). DG_4 simulates the generation of a renewable power source and for this reason its injected power is not controlled by the dispatch strategy. For this kind of sources it is expected a total injection of the available power, considering the intermittent nature of the renewable resources. The variable generation profile of $DG4$ affects the power balance of the controlled DGs as it can be seen in Fig. 12(b), where injected powers change in time. As it was discussed, the accuracy of the power dispatch is closely related to renewable generation forecasting. As can it be observed, the power-sharing remains accurate during all the OPs.

Reactive powers and voltages for the experimental test are presented in Fig. 13. Here it is possible to observe the impact that the MGCC failure has on the variables that depend directly on the CeCS. As the control over the V_{PCC} is lost, the voltage profile and the reactive powers reach operating points in disagreement with the control objectives (i.e., high values of e^{QD} and e^{V}). However, since the CoCS continues working, the system remains stable and once the CeCS is recovered, the control objectives are accurately reached again.

9.5 Test case 3: Communication impairments test

The third test was developed in order to evaluate the performance of the control strategy under certain communication impairments. The four DGs were implemented as controllable DGs, considering the CoCS ring scheme depicted in Fig. 9(b). The same active power load profile of test 2 was considered with a reactive power Q_L equal to zero during all the test (see Table 8).

Transmission periods of $T_V = 5$ s and $T_C = 0.5$ s were considered for CeCS and CoCS, respectively. Also, delays in the data reception were induced. Particularly, DG_2 was implemented with a reception delay of 0.3 s while DG_4 with a reception delay of 0.25 s. The results are presented in Fig. 14.

Active and reactive powers are presented in Fig. 14(a) and Fig. 14(b), respectively. Since these variables are related with the CoCS, the induced delays and the increase of the transmission period

Table 8 Loads for test 2

OP	OP1	OP2	OP3
P_L (main load)	1500 W	1500 W	1500 W
Local loads ($P_1 + P_2$)	0 W	1000 W	500 W
P_{TOTAL} ($P_L + P_1 + P_2$)	1500 W	2500 W	2000 W
Q_L (main load)	400 VAr	400 VAr	400 VAr
Q_{TOTAL}	400 VAr	400 VAr	400 VAr
Time interval	0 s≤t<20 s	20 s≤t<60 s	60 s≤t<100 s

T_C have a clear impact over the dynamics of the closed-loop system, as it can be seen in the loads changes at $t = 20$ s and $t = 60$ s. Although the delays increase the transient overshoots, the expected steady state values are reached in times that are not critical for the MG operation.

Voltages are presented in Fig. 14(c). These variables are related to the CeCS. The increase in the transmission period T_V affects the voltage recovery, as it can be seen in the load change at $t = 60$ s. However, after 5 s, once the updated CeCS data is sent, the voltages properly achieve the steady-state values and V_{PCC} reaches the control objective of 1 p.u.

Finally, it is worth noting that the values of the transmission periods and the delays induced in this test correspond to magnified scenarios. Even in this pessimistic scenario, the system presents good features in terms of control objectives achievement and dynamics performance.

10 Conclusion

This paper has presented a droop-free hierarchical control strategy that satisfies simultaneously several control objectives such as power-sharing, voltage regulation at PCC and optimal power dispatch. It is based on local modules implemented in each DG controller and a central module implemented in a MGCC, which uses a dual communication system to exchange data. A novel closed-loop small-signal model is presented. The resulting model is used for control parameters design guaranteeing the stability of the system. The selected tests allowed to evaluate the performance of the control strategy in different environments including normal operation and adverse conditions. The strategy presents excellent performance in terms of accomplishment of the control objectives and dynamics properties.

11 References

1 Vasquez, J.C., Guerrero, J.M., Miret, J., Castilla, M., García.De.Vicuña, L.: 'Hierarchical control of intelligent microgrids', *IEEE Ind Electronics Magazine*, 2010, **4**, (4), pp. 23–29

2 Bidram, A., Davoudi, A.: 'Hierarchical structure of microgrids control system', *IEEE Trans Smart Grid*, 2012, **3**, (4), pp. 1963–1976

3 Guerrero, J.M., Chandorkar, M., Lee, T., Loh, P.C.: 'Advanced control architectures for intelligent microgrids - part I: Decentralized and hierarchical control', *IEEE Trans on Ind Electron*, 2013, **60**, (4), pp. 1254–1262

4 Rocabert, J., Luna, A., Blaabjerg, F., Rodríguez, P.: 'Control of power converters in AC microgrids', *IEEE Trans Power Electron*, 2012, **27**, (11), pp. 4734–4749

5 Vergara, P.P., López, J.C., Rider, M.J., da Silva, L.C.P.: 'Optimal operation of unbalanced three-phase islanded droop-based microgrids', *IEEE Transactions on Smart Grid*, 2019, **10**, (1), pp. 928–940

6 Li, Z., Zang, C., Zeng, P., Yu, H., Li, S.: 'Fully distributed hierarchical control of parallel grid-supporting inverters in islanded AC microgrids', *IEEE Trans on Ind Informat*, 2018, **14**, (2), pp. 679–690

7 Vergara, P.P., Rey, J.M., Shaker, H.R., Guerrero, J.M., Jørgensen, B.N., da Silva, L.C.P.: 'Distributed strategy for optimal dispatch of unbalanced three-phase islanded microgrids', *IEEE Trans on Smart Grid*, 2018,

8 Bella, A.L., Cominesi, S.R., Sandroni, C., Scattolini, R.: 'Hierarchical predictive control of microgrids in islanded operation', *IEEE Trans on Autom Sci and Eng*, 2017, **14**, (2), pp. 536–546

9 Bidram, A., Davoudi, A., Lewis, F.L., Qu, Z.: 'Secondary control of microgrids based on distributed cooperative control of multi-agent systems', *IET Generation, Transmission Distribution*, 2013, **7**, (8), pp. 822–831

10 Shafiee, Q., Guerrero, J.M., Vasquez, J.C.: 'Distributed secondary control for islanded microgrids - a novel approach', *IEEE Trans Power Electron*, 2014, **29**, (2), pp. 1018–1031

11 Shafiee, Q., Stefanovic, C., Dragicevic, T., Popovski, P., Vasquez, J.C., Guerrero, J.M.: 'Robust networked control scheme for distributed secondary control of islanded microgrids', *IEEE Trans Ind Electron*, 2014, **61**, (10), pp. 5363–5374

12 Shrivastava, S., Subudhi, B., Das, S.: 'Distributed voltage and frequency synchronisation control scheme for islanded inverter-based microgrid', *IET Smart Grid*, 2018, **1**, (2), pp. 48–56

13 Lu, X., Yu, X., Lai, J., Guerrero, J.M., Zhou, H.: 'Distributed secondary voltage and frequency control for islanded microgrids with uncertain communication links', *IEEE Trans Ind Informat*, 2017, **13**, (2), pp. 448–460

14 Lou, G., Gu, W., Wang, L., Xu, B., Wu, M., Sheng, W.: 'Decentralised secondary voltage and frequency control scheme for islanded microgrid based on adaptive state estimator', *IET Generation, Transmission Distribution*, 2017, **11**, (15), pp. 3683–3693

15 Shafiee, Q., Nasirian, V., Vasquez, J.C., Guerrero, J.M., Davoudi, A.: 'A multi-functional fully distributed control framework for AC microgrids', *IEEE Trans on Smart Grid*, 2018, **9**, (4), pp. 3247–3258

16 Rey, J.M., Martí, P., Velasco, M., Miret, J., Castilla, M.: 'Secondary switched control with no communications for islanded microgrids', *IEEE Trans Ind Electron*, 2017, **64**, (11), pp. 8534–8545

17 Xia, Y., Peng, Y., Wei, W.: 'Triple droop control method for AC microgrids', *IET Power Electronics*, 2017, **10**, (13), pp. 1705–1713

18 Guerrero, J.M., Vasquez, J.C., Matas, J., García.De.Vicuña, L., Castilla, M.: 'Hierarchical control of droop-controlled AC and DC microgrids–A general approach toward standardization', *IEEE Trans Ind Electronics*, 2011, **58**, (1), pp. 158–172

19 Vasquez, J.C., Guerrero, J.M., Savaghebi, M., Eloy.Garcia, J., Teodorescu, R.: 'Modeling, analysis, and design of stationary-reference-frame droop-controlled parallel three-phase voltage source inverters', *IEEE Trans on Ind Electron*, 2013, **60**, (4), pp. 1271–1280

20 Savaghebi, M., Jalilian, A., Vasquez, J.C., Guerrero, J.M.: 'Secondary control scheme for voltage unbalance compensation in an islanded droop-controlled microgrid', *IEEE Trans Smart Grid*, 2012, **3**, (2), pp. 797–807

21 Sadeghkhani, I., Hamedani Golshan, M.E., Mehrizi-Sani, A., Guerrero, J.M.: 'Low-voltage ride-through of a droop-based three-phase four-wire grid-connected microgrid', *IET Generation, Transmission Distribution*, 2018, **12**, (8), pp. 1906–1914

22 Nutkani, I.U., Loh, P.C., Wang, P., Blaabjerg, F.: 'Cost-prioritized droop schemes for autonomous AC microgrids', *IEEE Trans Power Electron*, 2015, **30**, (2), pp. 1109–1119

23 Barklund, E., Pogaku, N., Prodanovic, M., Hernandez.Aramburo, C., Green, T.C.: 'Energy management in autonomous microgrid using stability-constrained droop control of inverters', *IEEE Trans on Power Electron*, 2008, **23**, (5), pp. 2346–2352

24 Li, Z., Zang, C., Zeng, P., Yu, H., Li, S.: 'Agent-based distributed and economic automatic generation control for droop-controlled AC microgrids', *IET Generation, Transmission Distribution*, 2016, **10**, (14), pp. 3622–3630

25 Li, Z., Zang, C., Zeng, P., Yu, H., Li, S.: 'Fully distributed hierarchical control of parallel grid-supporting inverters in islanded AC microgrids', *IEEE Trans Ind Informat*, 2018, **14**, (2), pp. 679–690

26 Xin, H., Zhang, L., Wang, Z., Gan, D., Wong, K.P.: 'Control of island AC microgrids using a fully distributed approach', *IEEE Trans on Smart Grid*, 2015, **6**, (2), pp. 943–945

27 Xin, H., Zhao, R., Zhang, L., Wang, Z., Wong, K.P., Wei, W.: 'A decentralized hierarchical control structure and self-optimizing control strategy for F-P type DGs in islanded microgrids', *IEEE Trans on Smart Grid*, 2016, **7**, (1), pp. 3–5

28 Wu, X., Chen, L., Shen, C., Xu, Y., He, J., Fang, C.: 'Distributed optimal operation of hierarchically controlled microgrids', *IET Generation, Transmission Distribution*, 2018, **12**, (18), pp. 4142–4152

29 Wu, X., Chen, L., Shen, C., Xu, Y., He, J., Fang, C.: 'Distributed optimal operation of hierarchically controlled microgrids', *IET Gen Trans Distrib*, 2018, **12**, (18), pp. 4142–4152

30 Savaghebi, M., Jalilian, A., Vasquez, J.C., Guerrero, J.M.: 'Secondary control for voltage quality enhancement in microgrids', *IEEE Trans Smart Grid*, 2012, **3**, (4), pp. 1893–1902

31 Etemadi, A.H., Davison, E.J., Iravani, R.: 'A generalized decentralized robust control of islanded microgrids', *IEEE Trans Power Syst*, 2014, **29**, (6), pp. 3102–3113

32 Kahrobaeian, A., Mohamed, Y.A.R.I.: 'Networked-based hybrid distributed power sharing and control for islanded microgrid systems', *IEEE Trans Power Electron*, 2015, **30**, (2), pp. 603–617

33 Nasirian, V., Shafiee, Q., Guerrero, J.M., Lewis, F.L., Davoudi, A.: 'Droop-free distributed control for AC microgrids', *IEEE Trans Power Electron*, 2016, **31**, (2), pp. 1600–1617

34 Nasirian, V., Shafiee, Q., Guerrero, J.M., Lewis, F.L., Davoudi, A. 'Droop-free team-oriented control for AC distribution systems'. In: 2015 IEEE Applied Power Electronics Conference and Exposition (APEC). (, 2015. pp. 2911–2918

35 Grünig, R., Kühn, R.: 'Process-based strategic planning'. (Springer Science & Business Media, 2011)

36 Ebner, D.: 'Formal and informal strategic planning: The interdependency between organization, performance and strategic planning'. (Springer Science & Business Media, 2013)

37 Guerrero, J.M., García de Vicuña, J.L., Matas, J., Castilla, M., Miret, J.: 'Output impedance design of parallel-connected UPS inverters with wireless load-sharing control', *IEEE Trans Ind Electron*, 2005, **52**, (4), pp. 1126–1135

38 Guerrero, J.M., Matas, J., García de Vicuña, J.L., Castilla, M., Miret, J.: 'Decentralized control for parallel operation of distributed generation inverters using resistive output impedance', *IEEE Trans Ind Electron*, 2007, **54**, (2), pp. 994–1004

39 Gamarra, C., Guerrero, J.M.: 'Computational optimization techniques applied to microgrids planning: A review', *Renewable and Sustainable Energy Reviews*, 2015, **48**, pp. 413 – 424

40 Garces, A.: 'A linear three-phase load flow for power distribution systems', *IEEE Trans on Power Systems*, 2016, **31**, (1), pp. 827–828

41 Wood, A.J., Wollenberg, B.F.: 'Power generation, operation, and control'. (John Wiley & Sons, 2012)

42 Matas, J., Castilla, M., Miret, J., García de Vicuña, J.L., Guzman, R.: 'An adaptive prefiltering method to improve the speed/accuracy tradeoff of voltage sequence detection methods under adverse grid conditions', *IEEE Trans Ind Electron*, 2014, **61**, (5), pp. 2139–2151

43 Kron, G.: 'Tensor analysis of networks', *New York*, 1939,

44 Dorfler, F., Bullo, F.: 'Kron reduction of graphs with applications to electrical networks', *IEEE Transactions on Circuits and Systems I: Regular Papers*, 2013, **60**, (1), pp. 150–163

45 Guo, X., Lu, Z., Wang, B., Sun, X., Wang, L., Guerrero, J.M.: 'Dynamic phasors-based modeling and stability analysis of droop-controlled inverters for microgrid applications', *IEEE Trans Smart Grid*, 2014, **5**, (6), pp. 2980–2987

46 Kabalan, M., Singh, P., Niebur, D.: 'Large signal Lyapunov-based stability studies in microgrids: A review', *IEEE Trans on Smart Grid*, 2017, **8**, (5), pp. 2287–2295

47 Boyd, S., El.Ghaoui, L., Feron, E., Balakrishnan, V.: 'Linear matrix inequalities in system and control theory'. vol. 15. (Siam, 1994)
48 Miret, J., García de Vicuña, J.L., Guzmán, R., Camacho, A., Moradi.Ghahderijani, M.: 'A flexible experimental laboratory for distributed generation networks based on power inverters', *Energies*, 2017, **10**, (10), pp. 1589
49 Fourer, R., Gay, D.M., Kernighan, B.W.: 'AMPL: A modeling language for mathematical programming'. 2nd ed. (Pacific Grove, CA: Brooks/Cole-Thomson Learning, 2003)
50 Wachter, A., Biegler, L.T.: 'On the implementation of an interior-point filter line-search algorithm for large-scale nonlinear programming', *Math Programming*, 2006, **106**, (1), pp. 25–57